Snowflake Divertor Configuration Effects on Pedestal Stability and Edge Localized Modes in NSTX and DIII-D.

V.A. Soukhanovskii[1], S.L. Allen[1], M.E. Fenstermacher[1], C.J. Lasnier[1], M.A. Makowski[1], A.G. McLean[1], D.D. Ryutov[1], F. Scotti[1], E. Kolemen[2], R.E. Bell[2], A. Diallo[2], S. Gerhardt[2], R. Kaita[2], S. Kaye[2], B.P. LeBlanc[2], R. Maingi[2], J.E. Menard[2], M. Podesta[2], R.J. Groebner[3], A.W. Hyatt[3], A.W. Leonard[3], T.H. Osborne[3], T.W. Petrie[3], R. Raman[4], and J.G. Watkins[5]

E-mail: vlad@llnl.gov

[1]Lawrence Livermore National Laboratory, 7000 East Ave, Livermore, CA 94550, USA
[2]Princeton Plasma Physics Laboratory, PO Box 451, Princeton, NJ 08543-0451, USA
[3]General Atomics, PO Box 85608, San Diego, CA 92186-5608, USA
[4]University of Washington, Seattle, WA 98195, USA
[5]Sandia National Laboratories, PO Box 969, Livermore, California 94551-0969, USA

Analyses of snowflake (SF) divertor [1] experiments in NSTX [2] and DIII-D [3] show that the SF divertor can increase magnetic shear and modify pressure profiles of the H-mode pedestal enabling pedestal stability control while maintaining good H-mode confinement (H_{98y2}~1). The scrape-off layer (SOL) and divertor geometry modifications lead to reduced peak temperature of plasma-facing components (PFCs) and reduced heat flux via partitioning and additional dissipation of ELM heat fluxes. The possibility of MHD stability and ELM control with the SF configuration was proposed theoretically [4] and impact of some SF properties on pedestal and ELMs has been studied with edge fluid and turbulence transport modeling [5-7]. Steady-state divertor heat flux mitigation in future tokamaks is envisioned via divertor magnetic and plate geometries and radiative scenarios. However, the unmitigated large ELMs with energy density up to 5-14 MJ-m^{-2} pose a significant risk for PFCs and motivate research on ELM mitigation and control [8].

The SF divertor configuration uses a second-order poloidal field null, or two nearby first order nulls, for a large region of low poloidal field B_p in the divertor [1]. Existing divertor coils have been used for steady-state SF divertor configurations in H-mode discharges in NSTX (I_p=0.9 MA, P_{NBI}=3-5 MW, and $B\times\nabla B$ down) and DIII-D (I_p=1.2 MA, P_{NBI}=3-5 MW, and $B\times\nabla B$ down). Previous analyses demonstrated inter-ELM heat transport manipulation and peak heat flux reduction in the SF divertor [2,3], whereas this work focuses on pedestal ELM stability and ELM heat transport and heat deposition on divertor PFCs.

The observed SF effects on pedestal and ELMs were different in NSTX and DIII-D, as the pedestal MHD stability depends on the pedestal stability operating point proximity to edge toroidal current density (peeling mode) and edge pressure gradient (ballooning mode) limits. Edge magnetic shear was increased by up to 30% in both NSTX and DIII-D discharges with SF divertors. In NSTX, pedestal stability operating point was close to the kink/peeling boundary with the standard divertor, and ELMs were stabilized by changes in pedestal pressure gradient and current density profile resulting from lithium conditioning [9]. With the SF divertor and lithium conditioning, large ELMs (f_{ELM}=12–35 Hz, $\Delta W_{MHD}/W_{MHD}$=5–10%) were destabilized. Initial profile analysis suggests that the pedestal was returned to pre-lithium conditions. Planned linear MHD stability calculations will help understand the destabilization mechanism. The large

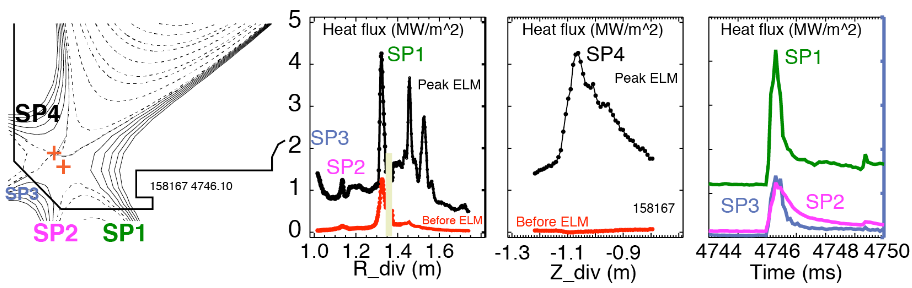

Figure 1 Divertor heat flux profiles and peak heat time histories in the attached near-exact SF divertor in DIII-D.

SF-induced ELMs led to reduced pedestal carbon concentration (by 30-50%), suggesting a way of controlling impurity accumulation in lithium-conditioned discharges. In DIII-D, kinetic profiles were weakly affected by the SF configuration [3]. The pedestal energy remained constant. A reduction in energy lost per ELM $\Delta W_{ELM}/W_{PED}$ by 5-15% was observed. ELM frequency was increased by 5-10%. The suggested mechanism is the reduction in the conduction loss channel with increased pedestal collisionality, in line with observed tokamak trends [8].

A reduction of ELM-induced divertor peak surface temperature T_{surf} (and heat flux) in the SF divertor (cf. standard divertor) was noted in both NSTX and DIII-D experiments [2,3]. A transient (ELM) heat pulse causes a divertor T_{surf} rise $\Delta T \sim \Delta W_{div}/(A\tau^{1/2})$, where ΔW_{div} is the total deposited energy, A is the ELM-wetted area, and τ is the deposition time [8]. The deposition time is proportional to the pedestal thermal ion transit time to the strike point $\tau_{||}=L_{mp\text{-}sp}/c_{ped}$, where c_{ped} is the ion sound speed. This time is proportional to the experimentally measured peak divertor heat rise time τ_{IR}. The transit time $\tau_{||}$ is typically longer in the SF geometry due to a greater connection length [2,3], the latter also resulting in a temporal dilution of the energy pulse and reducing its peak [4,6]. It is found that the divertor ELM energy density $\Delta W_{div}/A$ is also reduced, due to 1) a reduction of ΔW_{ELM}; 2) an increase of the ELM plasma-wetted area A; 3) a reduction of ΔW_{div} due to additional dissipative losses, especially pronounced in the high-density radiative divertor [2,3]; 4) partitioning ΔW_{div} / A between inner and outer targets and additional SF strike points, a key SF property [1]. These effects are illustrated in Fig. 1 and 2, where ELM heat flux temporal evolution (including τ_{IR}) and partitioning between additional SF strike points (SP) are shown in the near-exact SF configuration, and compared between the high-field side snowflake-minus and standard divertor in DIII-D. Greater (or nearly equal) ELM energy deposition is observed in the inboard divertor in DIII-D. A large ELM fraction is deposited outside of the divertor SOL on the outboard side (non-SP peaks in Fig. 2).

In summary, the SF divertor can modify pedestal and ELM characteristics via a larger area of low poloidal field in the divertor region and the associated modifications in magnetic geometry properties both inside and outside the separatrix, as demonstrated by the NSTX and DIII-D experiments. The modifications are generally beneficial and can be further developed into ELM control scenarios and ELM mitigation techniques.

This work is supported by the US DOE under DE-AC52-07NA27344, DE-AC02-09CH11466, DE-FC02-04ER54698, DE-FG02-07ER54917, and DE-AC04-94AL85000.

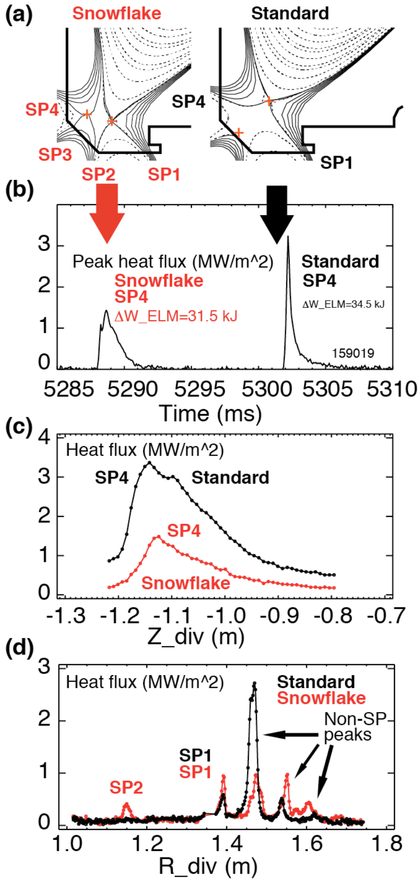

Figure 2 Comparison of ELMs in HFS SF-minus and standard attached divertors in DIII-D. (a) Magnetic equilibria; (b) Peak inner divertor heat flux time histories; (c) Vertical (inner) target and (d) horizontal target heat flux profiles.

[1] D.D. Ryutov, Phys. Plasmas 14 (2007) 064502; D. D. Ryutov and V. A. Soukhanovskii, Phys. Plasmas 22, 110901 (2015).
[2] V.A. Soukhanovskii et al., Nucl. Fus. 51 (2011) 012001; V.A. Soukhanovskii et al., Phys. Plasmas 19 (2012) 082504.
[3] S. Allen et al., paper PD/1-2, 2012 IAEA FEC, San Diego, CA, USA; D. N. Hill, Nucl. Fusion 53, 104001 (2013); V. A. Soukhanovskii et.al., Paper EX/7-4, IAEA FEC, 2014 St. Petersburg, Russia; V. A. Soukhanovskii et.al., J. Nucl. Mater. 463, 1191 (2015)
[4] D. D. Ryutov et. al., Paper TH/P4-18, IAEA FEC 2012, San Diego, CA, USA
[5] W.A. Farmer and D.D. Ryutov, Phys. Plasmas 20 (2013) 092117
[6] T. D. Rognlien et.al., J. Nucl. Mater. 438 (2013) S418–S421
[7] J. F. Ma et.al., Nucl. Fusion 54 (2014) 033011
[8] A. W. Leonard, Phys. Plasmas 21, 090501 (2014)
[9] R. Maingi et.al., Phys. Rev. Lett. 103, 075001 (2009); R. Maingi et al., Nucl. Fusion 52, 083001 (2012).